Y. Besel et alii, Frattura ed Integrità Strutturale, 35 (2016) 295-305; DOI: 10.3221/IGF-ESIS.35.34

Focussed on Crack Paths

Influence of joint line remnant on crack paths under static and fatigue loadings in friction stir welded Al-Mg-Sc alloy

Y. Besel, M. Besel, U. Alfaro Mercado
Institute of Materials Research, German Aerospace Center (DLR), Linder Hoehe, 51147 Cologne, Germany
yasuko.besel@dlr.de, michael.besel@dlr.de, Ulises.Alfaro@dlr.de

T. Kakiuchi, Y. Uematsu
Department of Mechanical Engineering, Faculty of Engineering, Gifu University, 1-1 Yanagido, Gifu 501-1193, Japan
kakiuchi@gifu-u.ac.jp, yuematsu@gifu-u.ac.jp

ABSTRACT. The influence of the joint line remnant (JLR) on tensile and fatigue fracture behaviour has been investigated in a friction stir welded Al-Mg-Sc alloy. JLR is one of the microstructural features formed in friction stir welds depending on welding conditions and alloy systems. It is attributed to initial oxide layer on butting surfaces to be welded. In this study, two different tool travel speeds were used. JLR was formed in both welds but its spatial distribution was different depending on the tool travel speeds. Under the tensile test, the weld with the higher heat input fractured partially along JLR, since strong microstructural inhomogeneity existed in the vicinity of JLR in this weld and JLR had weak bonding. Resultantly, the mechanical properties of this weld were deteriorated compared with the other weld. Fatigue crack initiation was not affected by the existence of JLR in all welds. But the crack propagated preferentially along JLR in the weld of the higher heat input, when it initiated on the retreating side. Consequently, such crack propagation behaviour along JLR could bring about shorter fatigue lives in larger components in which crack growth phase is dominant.

KEYWORDS. Friction Stir Weld (FSW); Joint line remnant (JLR); Lazy S; Zigzag line; Aluminium alloy; Fatigue.

INTRODUCTION

Conventionally, riveting has been used to join high strength aluminium plates for fuselage structures. For increasing demand towards improvement of energy consumption of an aircraft, weight reduction of a fuselage is one of the most effective solutions. As some material overlap is necessary for rivet joining, it is feasible to achieve weight reduction by replacing those rivet joints by welded butt joints. However, some aviation aluminum alloys such as precipitation hardening 2xxx and 7xxx series have poor weldability in case of fusion welding.
Friction stir welding (FSW) is solid state welding invented by TWI [1]. In the FSW processes, a non-consumable rotating tool consisting of cylindrical shoulder and pin is inserted into and moved along the butt joint line of two sheets. Frictional heating generated during this process causes softening of the material and local plastic deformation occurs. The plasticized material is stirred together by the rotation process resulting in a solid state join. Since the joining process by FSW basically

takes place well below the melting point of the joined materials, it can even be used to join such non-fusion-weldable aluminium alloys mentioned above.
Characteristics of the weld depend strongly on welding parameters such as tool rotating speed and tool travel speed. High strength joints without defects such as voids or lack of penetration (LOP) can be produced when using appropriate welding parameters [2, 3].
However, other types of weld imperfections or weld flaws can arise even under the optimized welding conditions, that may or may not compromise the integrity of the welded join. Especially at low heat input, a faint zigzag line is sometimes formed in the stir zone [4, 5]. Sato et al. revealed by TEM observation that this zigzag line comprised a high density of amorphous Al_2O_3 particles and suggested that they originated from the initial butt surfaces and its native oxide layer [6]. So, the zigzag line is also called "joint line remnant (JLR)" or "Lazy S". In the following, the term of JLR is used for this zigzag line microstructural feature in the weld. The intensity, spatial distribution and location of JLR depend mainly on the aluminium alloy system, welding parameters (esp. welding speed) and tool configuration. "Root flaw" (sometimes "kissing bond") is a weld defect with partially unwelded or only weakly bonded butt surfaces on the root side of the weld due to insufficient plunging of the tool, poor joint to tool alignment or inappropriate welding parameters [2, 7, 8, 9]. JLR can be formed accompanying root flaws depending on the welding conditions. These insufficient bonds at the bottom part of the JLR (i.e. root flaws) are not always detectable by non-destructive inspection but generally they open at root bend tests, while the JLR with sufficient root bonding does not deteriorate either root bending properties [4, 8] or tensile properties under as-welded conditions [10, 11]. Fatigue properties of the FS welds with JLR formation have been investigated for various Al alloys, e.g. 5083 and 6082 [8], 2024 and 5083 [12], 2024-T4 [13], 2198-T8 [14], and 1050-O [15]. Some researchers reported that kissing bonds or weak bonds on the root side caused fatigue crack initiation resulting in lower fatigue strengths [8, 12, 13]. In [14] and [15] it has been observed that fatigue fracture can take place independently from the existence of the JLR and cause hardly influence on fatigue strengths. Uematsu et al. investigated the fatigue initiation site in 1050-O with JLR and showed that localized plastic deformation at the boundary between TMAZ and HAZ at the advancing side of the FSW line caused fatigue crack initiation [15]. They also investigated fatigue behavior in FSWed samples of both heat-treatable and non-heat treatable alloys and concluded that fatigue fracture location was dependent on alloys due to their different microstructures and hardness distributions.
While FSW is a promising candidate as future joining technology, Al-Mg-Sc alloys are promising candidates as next baseline material for metallic fuselage structures. They have lower density and better corrosion resistance than conventional fuselage material, e.g. 2024, and they basically show good weldability [16]. The characteristic Al3Sc dispersoids in Al-Sc alloys show high thermal stability and act as recrystallization inhibitor [17]. Due to these thermally stable precipitations in Al-Mg-Sc alloys, they are expected not to have pronounced degradation of mechanical properties by FSW processing, which are generally found in heat-treatable 2XXX alloys without post-welding heat treatment. It has been demonstrated that the formation of joint line remnant and the mechanical integrity of the FSW joint are controlled by the welding parameters [4]. Consequently, in this study, the friction stir welding technique was applied to an Al-Mg-Sc alloy at two different tool travel speeds. Formation of the joint line remnant was examined, tensile and fatigue tests were performed and the influence of the JLR on the fracture behavior under tensile as well as fatigue loadings of the FSWed Al-Mg-Sc alloy was investigated.

EXPERIMENTAL PROCEDURES

The material used in this study was Al-Mg-Sc alloy 5024 –H116 plate with a nominal thickness of 3.3 mm. Its nominal chemical composition is listed in Tab. 1. The FSW tool consisted of a conical threaded pin (diameter 4.5 mm) and a cylindrical shoulder (diameter 12.5 mm). Two plates were butted and position-controlled friction stir welded at constant tool rotation speed of 1200 rpm. The surface of the plates to be welded was ground directly before the FSW process to remove the native oxide layer, and thus, minimize the influence of initial surface conditions on the joint quality. However, as a common matter of fact, an amorphous aluminum oxide film layer can be rapidly formed in laboratory air [18]. The tool travel speed was controlled at two levels: 480 and 720 mm/min (hereafter welds produced with these parameters are referred to as weld-480 and weld-720, respectively). Temperature during welding was monitored with a thermocouple plunged at 7 mm away from the joint line in the retreating side plate at a depth of 1 mm from the top surface. The root bending tests revealed no cracking, i.e. no root flaws were produced with those welding parameter sets.
Structural features of the welds including the JLR were examined with a light microscope on the polished cross sections etched with 5 wt% NaOH aqueous solution. Hardness profiles on the mid-section in the welds were measured by means of a micro-Vickers hardness tester under a load of 9.8 N.

For tensile tests, specimens with a parallel section length of 70 mm, a gauge length of 30 mm, width of 12 mm and nominal thickness of 3.3 mm were prepared (Fig.1). The weld center line passed through the center of the gauge length. The tensile tests were carried out at room temperature with the specimens as welded without removing any surface features of the weld such as weld flashes.

The geometry of the fatigue specimens is shown in Fig. 2. The weld center line lies perpendicularly to the loading direction in the center of the specimen. Tool marks and flashes formed by FSW on the surface were removed to eliminate their geometrical influence (e.g. notch effect) on crack initiation behavior. Prior to the fatigue tests, the specimen surfaces were mechanically polished with emery papers and finished with buff-polishing using 1µm-diamond suspension. The fatigue tests were carried out under cyclic loading conditions with a stress ratio of R = -1 at a frequency of 10 Hz.

Si	Fe	Cu	Zn	Mg	Mn	Ti	Sc	Al
0.25	0.4	0.2	0.2	3.9	0.25	0.2	0.4	Bal.

Table 1: Nominal chemical composition of Al-Mg-Sc alloy in wt%.

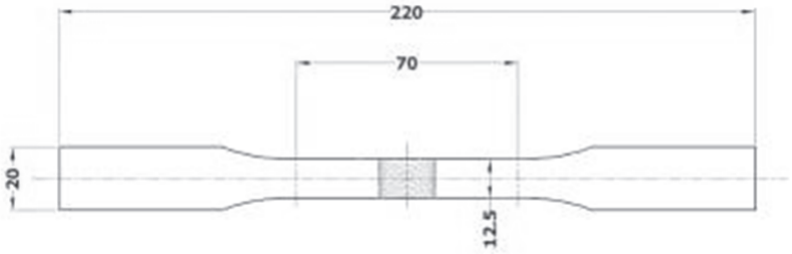

Figure 1: Tensile test specimen.

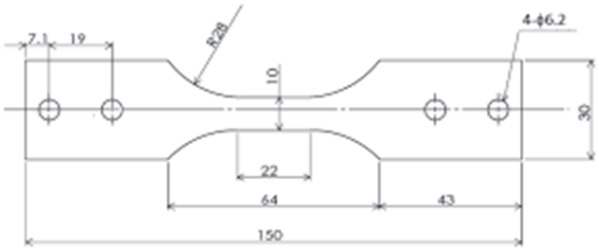

Figure 2: Fatigue test specimen.

RESULTS AND DISCUSSION

Weld structures

Fig. 3 shows optical micrographs of the cross sections of weld-480 and weld-720. In order to verify formation of JLR in those welds, stir-in-plate friction stir welding (one plate welding) was performed in Al-Mg-Sc plate with the tool travel speed of 600 mm/min. The macroscopic structure of the stir-in-plate weld is shown in Fig. 3(c). Dashed lines in the figures indicate the pin width. All welds had a stir zone (SZ) in the center surrounded by a thermo-mechanically affected zone (TMAZ). Fine recrystallized and equiaxed grains were formed in SZ around the weld center in all welds. Based on EBSD-measurements the average grain sizes in SZ of weld-480 and 720 were determined as 1.12 µm and 1.63 µm, respectively.

Obviously, no zigzag line was observed in the stir-in-plate weld, see Fig. 3(c). On the contrary, zigzag lines were observed in the butt weld for all weld conditions, as seen in Figs. 3(a) and (b), where the zigzag lines were highlighted with freehand lines for aid of visualization. Although the native oxide layer had been removed before the welding process, it seems that a new thin oxide film grew rapidly on the butting surfaces in laboratory air condition. This new oxide film was so thick that incomplete breakups remained resulting in formation of the zigzag line i.e. joint line remnant (JLR) in the welds. The degree of breakup of the oxide layer can sometimes be estimated based on the heat input during FSW [4, 5]. Generally, the heat input in FSW is considered to correlate with tool rotational speed and tool travel speed, where higher heat input is caused by higher tool rotational speed or lower tool travel speed, respectively [3, 19]. Consequently, in this study, the

higher heat input is expected for weld-480 than weld-720. Indeed, the maximum temperatures measured at 7 mm away from the joint line were 377 and 339 °C for weld-480 and weld-720, respectively.
The distribution of the JLR of weld-480 was wider on both advancing side (AS) and retreating side (RS) than that of weld-720. As marked with the rectangle I in Fig. 3(a), the JLR was extended towards the edge of SZ on the retreating side. In weld-720 (lower heat input), the JLR distributed more around the weld center in SZ (Fig. 3(b)). This spatial distribution of JLR serves as an indicator for the degree of material flow and mixing during the FSW process. Seidel and Reynolds visualized the material flow in the weld using marker insert technique and observed increased mixing in the weld with a decreasing weld pitch which is defined as the tool advance per rotation [20]. They suggested that the higher heat input might result in the softening of a greater amount of material, and consequently more material flow in the weld zone. In our study, comparing the distribution of the JLR in each weld, it can be said that greatest material flow was brought about in weld-480, i.e. higher heat input. This finding is consistent with the results of Seidel and Reynolds.

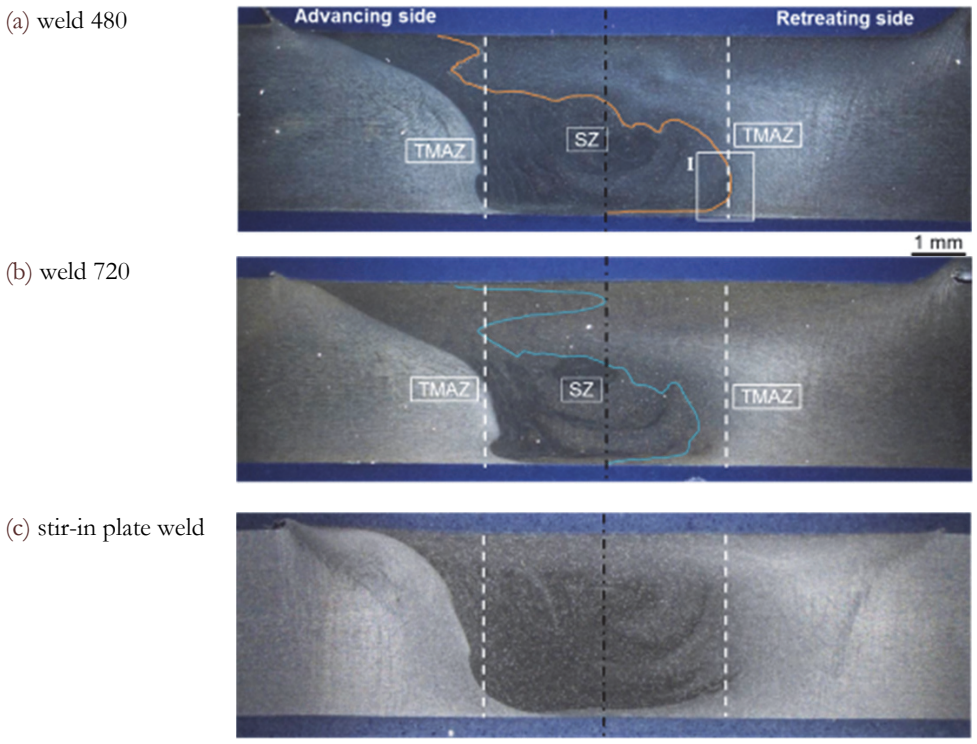

Figure 3: Macroscopic weld structure.

Hardness and tensile test results

Vickers hardness profiles of the different welds are shown in Fig. 4. In all weld conditions, softening occurred in SZ and hardness was mostly recovered in the neighboring TMAZ. The hardness in SZ of weld-720 was higher than that of the other two welds and the lowest hardness was observed in weld-480. This order reflects inversely the order of the heat input: i.e. higher heat input brought about greater softening in SZ.
Tensile test results are summarized in Tab. 2. Fracture occurred in SZ in all welds. Tensile strength and yield stress of weld-480 are lower than those of weld-720. In particular, the degradation in elongation of weld-480 is significant: the reduction is more than 30% compared to weld-720, although SZ (i.e. the fracture site) in weld-480 was softer than weld-720.

Weld ID	E-modulus [MPa]	0.2% yield stress $\sigma_{0.2}$ [MPa]	Tensile strength σ_{TS} [MPa]	Elongation ε_{max} [%]
weld-480	70793	218	311	4.61
weld-720	72182	237	329	6.77

Table 2: Tensile test results.

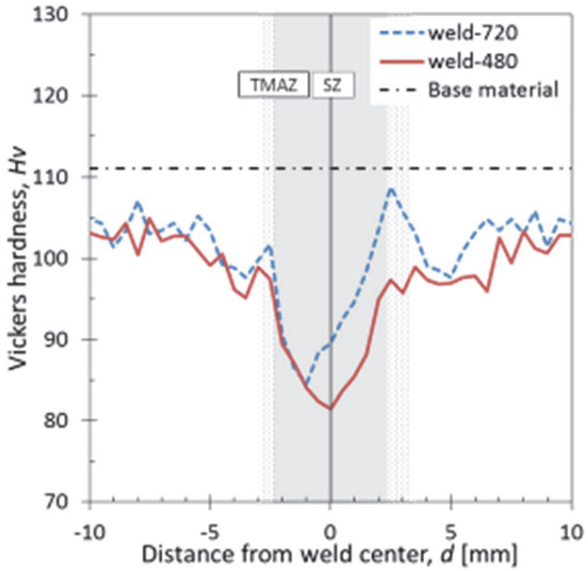

Figure 4: Hardness profiles along midsection of weld.

In order to identify fracture location of each weld, cross sections of the fractured samples were metallographically prepared, i.e. polished followed by etching. As clearly seen in Fig. 5, fracture behavior in weld-480 seems different from that in weld-720. While in weld-720 fracture occurred nearly through the center of the weld, weld-480 was fractured on the retreating side.

Fig. 6 shows the intersection of JLR and the fracture plane of weld-480 in more detail; the area corresponds to the dashed rectangle in Fig. 5(a). The fracture path in the lower part was smooth and steadily curved while the fracture face in the upper part was jagged but macroscopically nearly straight, see also upper part of fracture face in Fig. 5(a). The lower smooth fracture path presumably originated from JLR; as pointed by an arrow in Fig. 6 fracture face and JLR meet tangentially. Furthermore, taking into account the JLR spatial distribution in the weld seam (see Fig. 3(a)), it can be finally concluded that the fracture in the lower part took place along JLR. Scanning electron microscope (SEM) fractography was performed on the fracture surfaces in the upper and lower areas, as shown in Fig. 7(a) and (b), respectively. The SEM fractographs revealed different fracture behavior in both areas: comparably large dimples were observed in the upper area, while very finely shallow dimples covered the fracture surface in the lower area. The shallow dimples indicate low ductility or weak bonding. Since JLR was formed at the location of originally abutting free surfaces, it can be considered that the shallow dimples in the lower area were attributed to weak or incomplete bonding at JLR. Because more than about 30 % of the fracture path proceeded along JLR (lower part A-A' in Fig. 5(a)), weld-480 exhibited significantly lower elongation and strengths than the other welds showing JLR independent fracture paths.

Heat input in FSW is described to be proportional to tool rotational speed and inversely proportional to tool travel speed [3, 19]. It has been reported that high zigzag line pattern (herein JLR) is not formed in the high heat input welds, since degree of stirring increases with heat input and results in sufficient break-up of the initial oxide layer [4]. In this study, friction stir welding was performed at two different tool travel speed, i.e. two different heat input levels. JLR was formed in all welds, but the distribution of JLR in each weld was different. In the weld with the highest heat input (weld-480), the specimen was fractured partially along JLR which resulted in lower elongation than the other welds with lower heat input. Since the high heat input in weld-480 facilitated the material transport, the spatial distribution of JLR became wider. In the area where the fracture occurred, JLR located around the boundary of SZ and TMAZ, see Fig. 8, which corresponds to Area I marked with square in Fig. 3(a). Since the direct stirring of the material, fine-recrystallized, equiaxed grains were formed in SZ. Meanwhile, the material in TMAZ experienced strong shear deformation that resulted in a unique wavy structure as seen on the right-hand side in Fig. 8. Additionally, JLR at the fracture site lay almost normal to the loading direction and seemed to have comparably weak bonding properties. Furthermore, local inhomogeneity and mismatch of microstructure may induce local strain concentration under mechanical loading. As a consequence, it can be concluded that the fracture factually occurred along JLR in this area in weld-480 although higher heat input was applied than weld-720 not showing this kind of fracture along JLR.

(a) weld - 480

(b) weld - 720

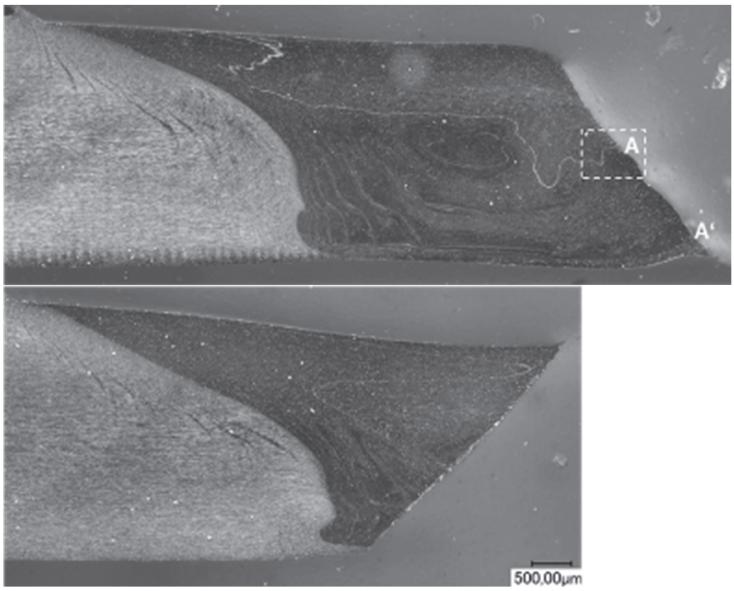

Figure 5: Cross sections of tensile fractured welds.

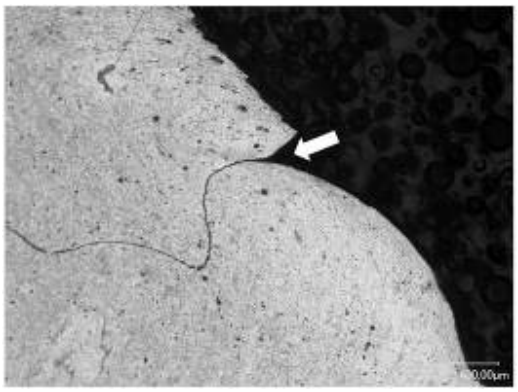

Figure 6: Magnified view of intersection of JLR and fracture surface (see dashed rectangle in Fig. 5)

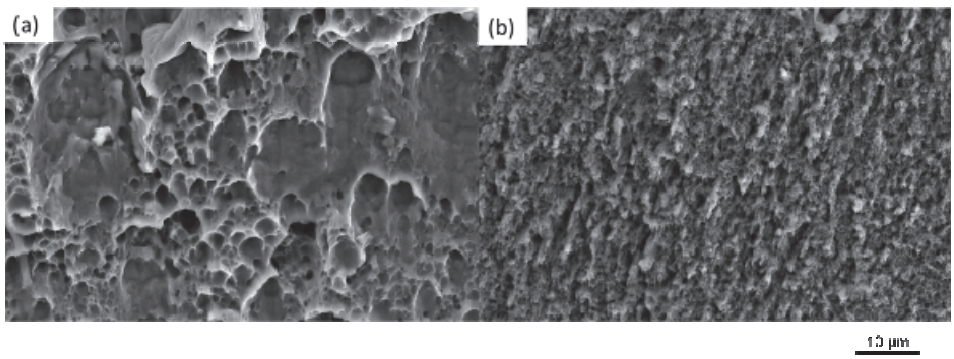

Figure 7: SEM fractographs of tensile fracture surface of weld-480: (a) upper part of weld, (b) lower part of weld along JLR.

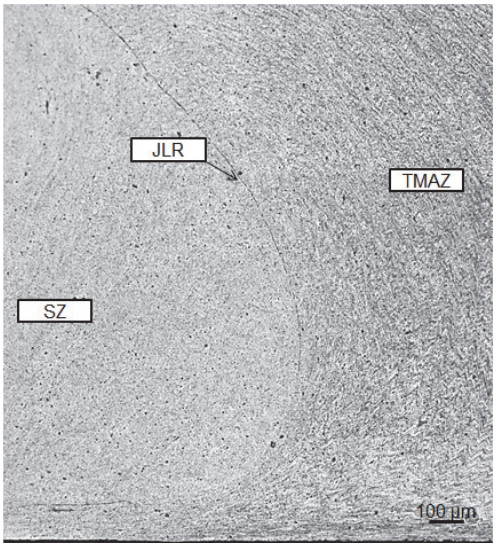

Figure 8: Micrograph of weld-480 in Area I of Fig. 3(a) around tensile fracture site.

Fatigue fracture behavior

S-N data of the FSW joints are drawn together with that of the base material in Fig. 9. Since the welds showed softening in all conditions, their fatigue lives were lower than the base material. Open marks indicate that fatigue crack initiation took place at weld defects. More details of the fatigue behavior of the FSWed Al-Mg-Sc alloy have been discussed somewhere else [21].

In this study, the focus is limited to the influence of JLR on the fatigue behavior. In weld-720, JLR didn't play any roles in either initiation or propagation behavior: i.e. fatigue cracks in those welds were initiated independently from the JLR distribution and their growth was not affected by JLR. In weld-480, fatigue crack initiation sites scattered around the weld both on the advancing side (AS) and retreating side (RS), as marked in Fig. 10. When a crack initiated on AS (at stress amplitudes σ_a = 240 MPa and 200 MPa), its propagation was also within AS and no influence of JLR was observed. Similarly, in the case of the crack initiation on RS (at stress amplitudes σ_a = 220 MPa and 180 MPa), the crack propagation was also in RS.

Fig. 11 shows SEM image of the fracture surface of the sample tested at σ_a = 220 MPa. The crack origin was located on the bottom surface as indicated with an arrow, and the crack grew from this origin radially towards the opposite top surface. Macroscopic crack growth directions according to the striation patterns on the fracture surface are indicated with several white arrows. Even after the crack reached the opposite surface of the specimen, the crack front trace was not parallel to the through-thickness direction as it is typically observed for through-thickness cracks in homogeneous material under tensile cyclic loading.

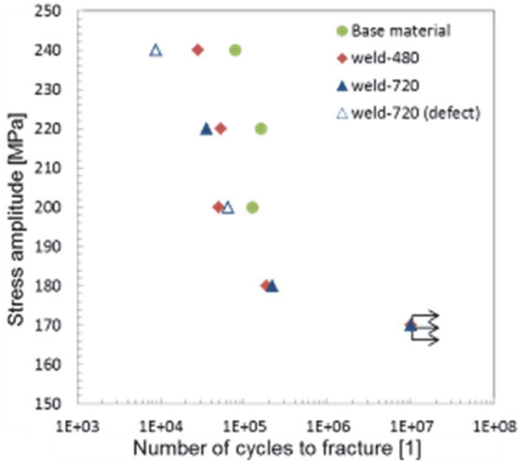

Figure 9: Fatigue data of friction stir welds and base material (*R*=-1).

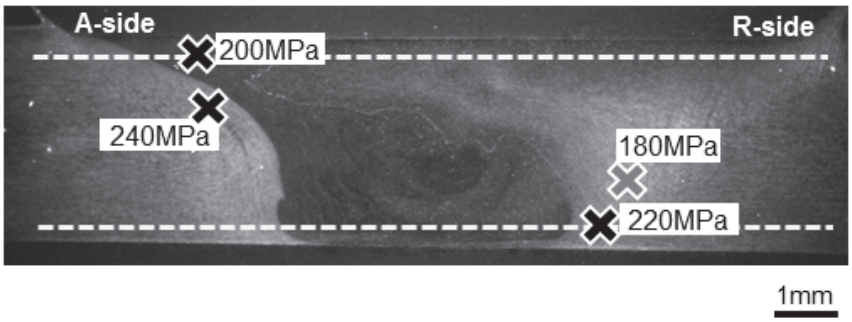

Figure 10: Fatigue crack initiation sites of weld-480.

Irregular fracture morphology was observed in the lower and left-hand part of the specimen. In order to investigate the fatigue crack growth behavior on this irregular fracture, a cross section at B-B' was examined, as shown in Fig. 12. Macroscopically large flexure was observed on this cross section (Fig. 12(a)). The profile C-C' corresponds to the irregular fracture site (see Fig. 11). JLR was well pronounced in this cross section, and the crack encountered JLR. As seen in the enlarged image (Fig. 12(b)) of the rectangle in Fig. 12(a), it can be observed that the crack propagation partially occurred along JLR. This area was nearly consistent with the fracture site along JLR in the tensile test as mentioned in the previous section (see Fig. 8). Thus, also fatigue crack propagation partially along JLR resulted in macroscopic flexure of the crack path.

SEM fractography was performed for more detailed observation in the areas marked by the rectangles II in Fig. 11. Fig.s 13(a) shows Area II where the irregular fracture began to appear. The lower part of the image displays the irregular fracture surface, i.e. JLR-fracture site, see arrow (1). In the upper part fine striations were observed with intervals of a few micrometers. Major crack propagation direction in this area was upwards according to the orientation and the development of intervals of the striations, see arrow (2), and it indicates that the crack propagated from the JLR-fracture. Fig. 13(b) shows higher magnification image of Area III marked in Fig. 13(a). No striation was observed in the JLR-fracture part (lower part of Fig. 13(b)). Instead, very fine asperity was formed. Since the asperity of JLR fracture in the lower part of Fig. 13(b) was equivalent to the average grain size of weld-480 (1.67 μm), it is considered that the crack propagated intergranularly at JLR.

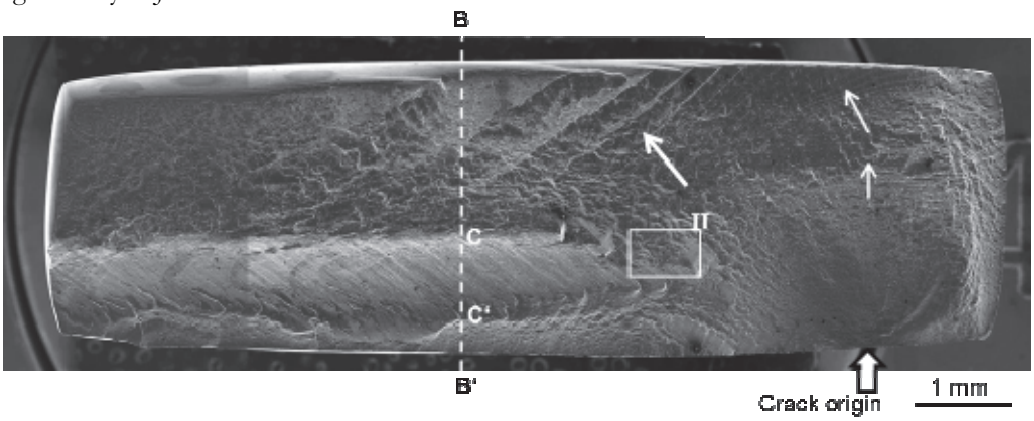

Figure 11: Fatigue fracture surface of weld-480 tested at σ_a = 220 MPa.

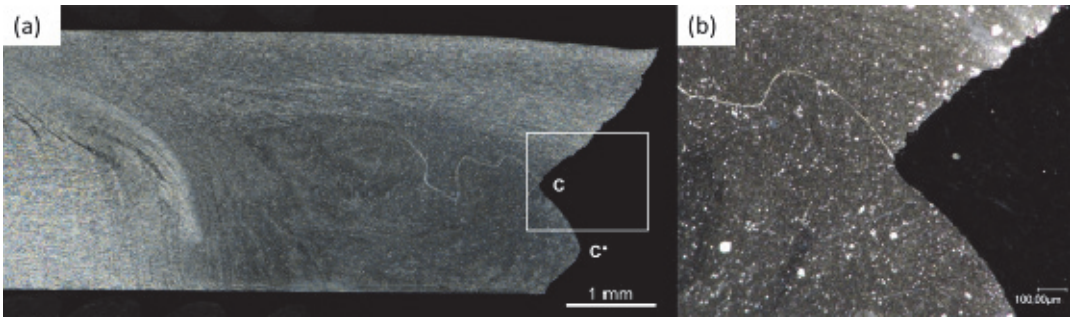

Figure 12: Cross section at B-B' in Fig. 11: (a) macrograph, (b) magnified view of the area defined by the rectangle in (a).

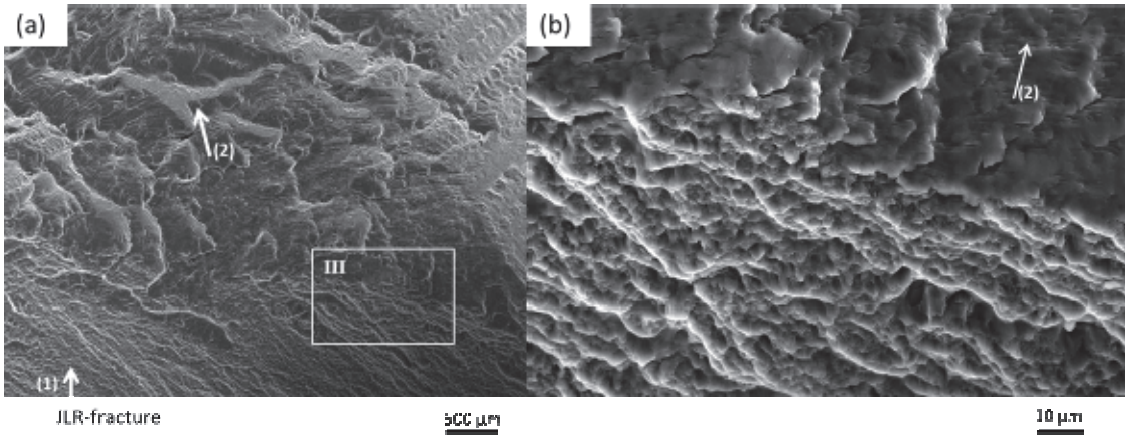

Figure 13: SEM observation of fatigue fracture surface of weld-480: (a) Magnified view of Area II in Fig. 11, (b) magnified view of Area III.

Based on the evidence of the crack growth direction in the surrounding matrix as seen in Fig. 13(b), it can be concluded that when the crack approached there the fatigue crack propagated preferentially at JLR because of its weak bonding, and grew further from the JLR-fracture site into the matrix. As a result, the macroscopic crack growth direction in this area became not totally perpendicular to the through-thickness direction as seen in Fig. 11. The fine dimples in Area VII of JLR-fracture surface in the residual fracture regime resembled the monotonic tensile fracture as seen in Fig. 7(b). Taking into account the elevated net stress in this section due to the already long through-thickness crack, it can be concluded that the weakly bonded JLR was ruptured quasi-statically. Thus, when the fatigue crack approached JLR, it propagated firstly at JLR and then into the matrix. The fracture area at JLR was about 10% of the total fracture surface. The locally weak bonding clearly accelerated local crack growth rate around JLR.
However, significant decrease in fatigue life of the two specimens where JLR-fracture occurred on RS was not observed as seen in Fig. 9. It is generally known that most part of fatigue lives of a metallic component is spent on initiation and early propagation phases. The fracture at JLR occurred in the phase of comparably fast striation growth as seen in Fig. 13. Therefore, the crack propagation at JLR could shorten the fatigue life to some extent but its contribution to the total life was insignificant in the laboratory size specimens used in this study. In contrast, when the component is large, i.e. crack propagation phase may occupy a significant amount of fatigue life, the crack growth along JLR could lead to significantly shorter life time of such components.

SUMMARY AND CONCLUSIONS

Influence of joint line remnant (JLR) in friction stir welded (FSWed) Al-Mg-Sc alloy on tensile and fatigue fracture behavior was investigated. Butt welding was performed under two different heat input conditions by changing tool travel speeds. Fatigue tests were conducted with polished specimens, i.e. without welding flash and root flaws. Although the native oxide layer was removed before FS welding, a new oxide layer was immediately formed under lab air condition. This newly generated oxide layer was thick enough to form pronounced JLR in the welds. The distribution of JLR in the welds clearly were differed by the heat input levels: In the lower heat input weld, JLR distributed mainly around the weld center. Higher heat input facilitated the material flow during the welding process, and consistently JLR in the weld with the high heat input was more widely distributed and reached the boundary of stir zone (SZ) and thermo-mechanically affected zone (TMAZ) on retreating side (RS) of the weld, where microstructural mismatch exists. When JLR located within SZ, tensile fracture occurred independently of the existence of JLR. However, because of the local microstructural mismatch between SZ and TMAZ existing at JLR in addition to weak bonding of JLR, tensile fracture occurred partially along JLR in the higher heat input weld. As a result, this weld showed lower yield and tensile strengths and less ductility than the other weld.
Fatigue crack initiation was not influenced by JLR in all welds. But in the higher heat input weld, when a crack initiated on RS and approached JLR, the fatigue fracture occurred preferentially along JLR. Due to the weak bonding, the fatigue crack propagated intergranularly at JLR. Contribution of this preferential fatigue crack growth at JLR towards the total fatigue life was insignificant because it happened in the striation growth stage in a comparably small specimen. In the case that the fatigue crack growth phase contributes significantly to fatigue lives, i.e. in large components under moderate

fatigue loading, the effect of JLR on crack growth rates as well as the applicability of linear elastic fracture mechanics and e.g. its K-concept should be investigated.

ACKNOWLEDGEMENT

The authors would like to express their sincere gratitude to the Japanese Society for the Promotion of Science for funding most of this work under the "JSPS Postdoctoral Fellowship (Short-Term) for North American and European Researchers" (FY 2012). Further thanks to the colleagues from the Institute for Materials Research of the German Aerospace Center in Cologne, namely Mr. Sauer for providing the FSW joints and Mr. Fuchs for mechanical testing.

REFERENCES

[1] Thomas, W. M., Nicholas, E. D., Needham, J. C., Murch, M. G., Temple-Smith, P., Dawes, C. J, Improvements relating to friction welding. European Patent Specification EP 0 615 480 B1, (1992).
[2] Leonard, A.J., Lockyer S.A., Flaws in friction stir welds, Proc. of 4th Int. Symposium on Friction Stir Welding, Park City, Utah, USA, (2003).
[3] Kim, Y.G., Fujii, H., Tsumura, T., Komazaki, T., Nakata, K., Three defect types in friction stir welding of aluminum die casting alloy, Mat. Sci. Eng. A, A415 (2006) 250–254.
[4] Sato, Y.S., Takauchi, H., Park, S.H.C., Kokawa, H., Characteristics of the kissing-bond in friction stir welded Al alloy 1050, Mater. Sci. Eng. A, A405 (2005) 333–338.
[5] Peel, M., Steuwer, A., Preuss, M., Withers, P.J., Microstructure, mechanical properties and residual stresses as a function of welding speed in aluminium AA5083, Acta Mater., 51 (2003) 4791–4801.
[6] Sato, Y.S., Yamashita, F., Sugiura, Y., Park, S.H.C., Kokawa, H., FIB-assisted TEM study of an oxide array in the root of a friction stir welded aluminium alloy, Scripta Mater., 50 (2004) 365–369.
[7] Oosterkamp, A., Oosterkamp, L.D., Nordeide, A., 'Kissing Bond' Phenomena in Solid-State Welds of Aluminum Alloys, Welding Journal, 83, (2004) 225–231.
[8] Dickerson, T.L., Przydatek, J., Fatigue of friction stir welds in aluminium alloys that contain root flaws, Int. J. of Fatigue, 25 (2003) 1399–1409.
[9] Vugrin, T., Schmuecker, M., Staniek, G., Root Flaws of Friction Stir Welds – an Electron Microscopy Study, in K.V. Jata et al. (ed.): Friction Stir Welding and Processing III, The Minerals, Metals and Materials Society, 2005, pp. 277-284.
[10] Liu, H.J., Chen, Y.C., Feng, J.C., Effect of zigzag line on the mechanical properties of friction stir welded joints of an Al-Cu alloy, Scripta Mater., 55 (2006) 231–234.
[11] Ren, S.R., Ma, Z.Y., Chen, L.Q., Effect of initial butt surface on tensile properties and fracture behavior of friction stir welded Al-Zn-Mg-Cu alloy, Mater. Sci. Eng. A, A479 (2008) 293–299.
[12] Zhou, C., Yang, X., Luan, G., Effect of oxide array on the fatigue property of friction stir welds, Scripta Mater., 54 (2006) 1515–1520.
[13] Di, S., Yang, X., Luan, G., Jian, B., Comparative study on fatigue properties between AA2024-T4 friction stir welds and base materials, Mater. Sci. Eng. A, A435–436 (2006) 389-395.
[14] Jolu, T.L., Morgeneyer, T.F., Gourgues-Lorenzon, A.F., Effect of joint line remnant on fatigue lifetime of friction stir welded Al-Cu-Li alloy, Science and Technology of welding and joining, 15 (2010) 694–698.
[15] Uematsu, Y., Tokaji, K., Shibata, H., Tozaki, Y., Ohmune, T., Fatigue behavior of friction stir welds without neither welding flash nor flaw in several aluminium alloys, Int. J. of Fatigue, 31 (2009) 1443–1453.
[16] Filatov, Y.A., Yelagin, V.I., Zakharov, V.V., New Al-Mg-Sc alloys, Mater. Sci. Eng. A, A280 (2000) 97–101.
[17] Riddle, Y.W., Sanders, T.H., A study of coarsening, recrystallization, and morphology of microstructure in Al-Sc-(Zr)-(Mg) alloys, Metall. Mater. Trans. A, 35A (2004) 341–350.
[18] Michel, S.A., Oxidation and fatigue crack growth in aluminium alloys, Proc. of 3rd Int. Conf. Microscopy of Oxidation, Cambridge UK, (1996).
[19] Frigaard, O., Grong, O., Mildling, O.T., A Process Model for Friction Stir Welding of Age Hardening Aluminum Alloys, Metall. Mater. Trans A, 32A (2001) 1189–1200.

[20] Seidel, T.U., Reynolds, A.P., Visualization of the Material Flow in AA2195 Friction-Stir Welds Using a Marker Insert Technique, Metal. Mater. Trans. A, 32A (2001) 2879–2884.
[21] Besel, M., Besel, Y., Alfaro Mercado, U., Kakiuchi, T., Uematsu, Y., Fatigue behavior of friction stir welded Al-Mg-Sc alloy, Int. J. Fatigue, 77 (2015) 1-11. doi: 10.1016/j.ijfatigue.2015.02.013.